Journal of Solid State Chemistry 184 (2011) 2190–2195

Contents lists available at ScienceDirect

Journal of Solid State Chemistry

journal homepage: www.elsevier.com/locate/jssc

$W_{18}O_{49}$ nanorods decorated with Ag/AgCl nanoparticles as highly-sensitive gas-sensing material and visible-light-driven photocatalyst

Shibin Sun [a], Xueting Chang [b,*], Lihua Dong [b], Yidong Zhang [c], Zhenjiang Li [a,*], Yanyan Qiu [a]

[a] College of Electromechanical Engineering, Qingdao University of Science and Technology, Qingdao 266061, People's Republic of China
[b] Institute of Marine Materials Science and Engineering, Shanghai Maritime University, Shanghai 200135, People's Republic of China
[c] Institute of Surface Micro and Nano Materials, Xuchang University, XuChang 461000, People's Republic of China

ARTICLE INFO

Article history:
Received 10 December 2010
Received in revised form
11 March 2011
Accepted 21 June 2011
Available online 29 June 2011

Keywords:
$Ag/AgCl/W_{18}O_{49}$ NRs
Photochemical
Gas-sensing properties
Photocatalyst

ABSTRACT

A novel gas-sensing material and photocatalyst was successfully obtained by decorating Ag/AgCl nanoparticles on the $W_{18}O_{49}$ nanorods through a clean photochemical route. The as-prepared samples were characterized using combined techniques of X-ray diffractometry, electron microscopy, energy dispersive X-ray spectrometry, and X-ray photoelectron spectroscopy. Gas-sensing measurements indicate that the $Ag/AgCl/W_{18}O_{49}$ NRs sensors exhibit superior reducing gas-sensing properties to those of bare $W_{18}O_{49}$ NRs, and they are highly selective and sensitive to NH_3, acetone, and H_2S with short response and recovery times. The $Ag/AgCl/W_{18}O_{49}$ NRs photocatlysts also possess higher photocatalytic performance than bare $W_{18}O_{49}$ NRs for degradation of methyl orange under simulated sunlight irradiation. Possible mechanisms concerning the enhancement of gas-sensing and photocatalytic activities of the $Ag/AgCl/W_{18}O_{49}$ NRs composite were proposed.

1. Introduction

Semiconductor oxides are important for many environmental and energy issues because, they cannot only utilize solar energy to eliminate harmful pollutants present in air and water but also effectively detect toxic and hazardous gases as well as biological species [1–4]. The demands for new types of photocatalysts, and gas and biosensors with enhanced functionalities are the driving forces for both fundamental and applied researches in the area of semiconductor-oxide-related nanotechnology. To date, various semiconductor oxides including ZnO [5], TiO_2 [6], WO_3 [7], In_2O_3 [8], CuO [9], Cr_2O_3 [10], and SnO_2 [11] have been prepared, and their photocatalytic and gas and biosensing properties have also been widely investigated by many research groups around the world.

Among a diverse of semiconductor oxides, tungsten oxides have attracted much recent interest due to their unique physical, chemical, and optical properties. Tungsten oxide nanocrystals, varies in shape, size and structure, are potential gas-sensing materials for both oxidizing gases such as NO_2 [12] and reducing gases such as H_2S [13], NH_3 [14], acetone [15], and ethanol [7,16]. They have also been found to be potential photocatalysts for decomposing organic compounds [17]. However, the sensitivities of the reported tungsten oxide-based sensors are not high enough for practical application and need to be improved. In addition, it has been reported that pure tungsten oxides, e.g. WO_3, have a lower light energy conversion efficiency than TiO_2 as the reduction potential of the electrons in WO_3 is low due to its low conduction band level [18]. Recent researches reveal that, coupling of tungsten oxide nanostructures and their related compounds with other semiconductors or metals could improve their photocatalytic and sensing properties. For example, Pt-loaded nanowires [18], Pt-loaded nanoporous-walled WO_3 nanotubes [19], Pt-loaded WO_3 nanoparticles [20], Au-activated WO_3 nanorods [21], Au-doped WO_3 powders [22], Ag-loaded mesoporous WO_3 [23], and Cr-doped WO_3 nanoparticles [24] were proven to exhibit superior gas-sensing or photocatalytic performances than those of bare WO_3 nanomaterials.

Plasmonic photocatalysts, which consist of Ag metal with strong surface plasmon resonance and semiconductors Ag*X* (*X*=Cl, Br, I), are attracting more recent attentions because of their excellent photocatalytic activities under visible light irradiation [25–28]. Additionally, oxide semiconductors or their related compounds decorated with plasmonic photocatalysts, such as $Ag/AgBr/WO_3 \cdot H_2O$ nanostructures [29], $Ag/AgCl/TiO_2$ nanotube arrays [30], and $AgBr/Ag/Bi_2WO_6$ nanojunction [31], were also found to exhibit improved photocatalytic activities for the destruction of bacteria and for the degradation of organic dye than bare semiconductors. To date, however, there has been no report on the decoration of non-stoichiometric tungsten oxides (usually expressed as WO_x, $2 \le x < 3$) with other semiconductors, noble metals or the novel plasmonic photocatalysts. Compared with WO_3, the intrinsic oxygen vacancies in the WO_x ($2 \le x < 3$) could offer more active sites for holding other metals or semiconductors.

* Corresponding authors.
E-mail addresses: xuetingchang@yahoo.cn (X. Chang), zj126@126.com (Z. Li).

0022-4596/$ - see front matter © 2011 Elsevier Inc. All rights reserved.
doi:10.1016/j.jssc.2011.06.024

In this paper, further extending from the successful synthesis of $W_{18}O_{49}$ nanorods through solvothermal method with WCl_6 as a precursor and cyclohexonal as a solvent, Ag/AgCl nanoparticle-loaded $W_{18}O_{49}$ nanorods (Ag/AgCl/$W_{18}O_{49}$ NRs) were obtained using a clean photochemical technique. By introducing the Ag or Ag^+ into the system, we aim to design new material with functionalized properties using the 1-D nanostructured $W_{18}O_{49}$ as a template. The resulting Ag/AgCl/$W_{18}O_{49}$ NRs were found to exhibit better gas-sensing and photocatalytic properties than those of bare $W_{18}O_{49}$ NRs.

2. Experimental details

2.1. Preparation of Ag/AgCl/$W_{18}O_{49}$ nanorods

The preparation of Ag/AgCl nanoparticles decorated $W_{18}O_{49}$ nanorods involves two steps: the first step is the synthesis of $W_{18}O_{49}$ nanorods ($W_{18}O_{49}$ NRs) using a simple solvothermal method with tungsten hexachloride (WCl_6, 99.9%, Aladdin-Reagent) as a precursor and cyclohexanol as a solvent, and the second is the loading of Ag/AgCl nanoparticles on the resulting nanorods.

The preparation of $W_{18}O_{49}$ NRs has been reported in our previous work in detail [32]. Typically, WCl_6 were firstly dissolved in 2 ml of ethanol in a beaker to obtain a solution, which was then transferred into a Teflon-lined high-pressure reaction vessel of 100 mL capacity. Cyclohexanol were then added to the vessel. The reaction vessel was finally sealed and heated at 200 °C in a Muffle furnace for 8 h. After natural cooling to room temperature, the as-synthesized products were washed thoroughly with distilled water several times, and finally centrifuged with distilled water, ethanol and acetone, respectively.

Ag/AgCl nanoparticle decorated $W_{18}O_{49}$ nanorods (Ag/AgCl/$W_{18}O_{49}$ NRs) were prepared by the photochemical route in a photochemical reactor (XPA-7, Xujiang Electromechanical Plant). An ethanol solution of silver nitrate ($AgNO_3$, 99.8%, China National Medicine Corparation Ltd.) was firstly prepared by dissolving 0.02 g of $AgNO_3$ into 60 mL ethanol. 0.10 g of $W_{18}O_{49}$ nanorods was then added to the ethanol solution. The ethanol suspension containing the $W_{18}O_{49}$ nanorods and $AgNO_3$ was subsequently exposed to mimic daylight provided by a 300 W Xe lamp under magnetic stirring. During the irradiation processing, small amount of dilute hydrochloric acid was added dropwise. After 2 h of irradiation, the solution color changed from blue to silver gray, and the Ag/AgCl/$W_{18}O_{49}$ NRs were obtained. The Ag/AgCl/$W_{18}O_{49}$ NRs were finally separated from the suspension after centrifuging at 8000 rpm for 5 min for further examination.

2.2. Characterization

The crystalline structure, morphology, chemical composition and surface features of the as-synthesized samples were characterized by X-ray diffraction (XRD, D/MAX-2500, Cu radiation), energy dispersive X-ray spectroscopy (EDS), transmission electron microscopy (TEM, JEOL 2000FX, operated at 120 kV), high magnification transmission electron microscopy (HRTEM, JEOL JEM 2100, operated at 200 kV), and X-ray photoelectron spectrometry (XPS, PHI 5300, Mg kR X-ray source, 1253.6 eV).

2.3. Gas-sensing tests

The gas-sensing activities of the Ag/AgCl/$W_{18}O_{49}$ NRs sensor towards various flammable vapors including acetone, 93# gasoline and ethanol, and harmful gases such as ammonia and hydrogen sulfide were evaluated through a WS-30 A system (Weisheng Electronics Co. Ltd., China). The preparation process of the gas sensors was as follows. Firstly, powders of Ag/AgCl/$W_{18}O_{49}$ NRs were mixed with glycerol to form a paste. The paste was then coated on a ceramic tube with a pair of Au electrodes covered by Pt wires, and then dried at 100 °C for 10 min. The Ag/AgCl/$W_{18}O_{49}$ NRs sensor schematic and the equivalent circuit of the testing system are shown in Fig. S1. The response time is defined as a duration in which the voltage rises to 90% of the equilibrium value since the gas is injected, and conversely, the recovery time is defined as a duration in which the voltage decreases to 10% of the equilibrium value since the gas is released. The sensitivities of the Ag/AgCl/$W_{18}O_{49}$ NRs sensor to different objects were calculated from the equation of $S=R_{air}/R_{gas}$, where R_{air} and R_{gas} are the resistances of the Ag/AgCl/$W_{18}O_{49}$ NRs sensor in air and in detected gases, respectively. As shown in Fig. S1b, the Ag/AgCl/$W_{18}O_{49}$ NRs sensor encases a load resistor (R_f) with known resistance, and a source voltage of 5 V (U_0) is applied on the circuit. The output voltage (U_{out}) on R_f can be measured by the system, and the resistances (R_{air} and R_{gas}) of the sensors can be therefore calculated based on the equation of $R=U_0-U_{out}/U_{out}R_f$.

2.4. Photocatalytic evaluation

Photocatalytic activities of the Ag/AgCl/$W_{18}O_{49}$ NRs were evaluated by degradation of methyl orange (MO) in an aqueous solution under simulated daylight irradiation provided by a 350 W Xe lamp. Photodegradation of MO was carried out in a photochemical reactor containing a suspension of the Ag/AgCl/$W_{18}O_{49}$ NRs photocatalysts (50 mg) in a MO aqueous solution (50 mL, 10 mg/L) with continuing agitation using a magnetic stirrer. Prior to the light irradiation, the MO solutions with the photocatalysts were kept in dark for 2 h to reach an adsorption–desorption equilibrium. The absorbance of MO solutions before and after degradation by the photocatalysts was analyzed by UV–*vis* diffuse reflectance spectroscopy (U-3010, HITACHI). The concentration of MO in aqueous solution was simply determined by the maximum absorption measurement (around 465 nm of wavelength). The photocatalytic efficiency of MO over different photocatalysts is defined by the equation of $C_0-C/C_0100\%$, where C is the concentration of MO aqueous solution after light irradiation, and C_0 is the equilibrium concentration of MO at the equilibrium adsorption state Simultaneously, Ag/ZnO nanoparticles (NPs) with diameters of about 20 nm prepared by a coprecipitation method and bare $W_{18}O_{49}$ NRs were chosen as reference samples.

3. Results and discussions

3.1. Characterization of Ag/AgCl/$W_{18}O_{49}$ NRs

Fig. 1 shows the XRD patterns of the pure $W_{18}O_{49}$ NRs and the Ag/AgCl/$W_{18}O_{49}$ NRs. The main diffraction peaks of XRD pattern of pure $W_{18}O_{49}$ NRs can be well indexed with monoclinic $W_{18}O_{49}$ (JCPDS file 71-2450). The strongest peak intensity of (0 1 0) plane indicates that the ⟨0 1 0⟩ is the dominant growth direction of the $W_{18}O_{49}$ NRs. After photochemical process, apparent diffraction peaks corresponding to AgCl and Ag can be observed, suggesting the successful decoration of AgCl and Ag onto the $W_{18}O_{49}$ NRs, as shown in Fig. 1b. EDS analysis (Fig. S2) also reveals that the resulting products are composed of elements of W, O, Ag, and Cl. The diffraction peaks at 27.8°, 32.2° and 46.2° can be assigned to (1 1 1), (2 0 0) and (2 2 0) planes of the cubic phase of AgCl, respectively (JCPDS file 31-1238); while peaks at 38.1°, 44.3° and 64.4° can be assigned to (1 1 1), (2 0 0) and (2 2 0) crystal orientations of the cubic phase of Ag, respectively (JCPDS file 65-2871).

Bundled $W_{18}O_{49}$ nanowires/nanorods were synthesized through a simple solovothermal method using WCl_6 as the raw

material [32]. Fig. 2a shows a low magnification TEM image of the Ag/AgCl/$W_{18}O_{49}$ NRs prepared by the photochemical method. It is clear that the bundled feature of the original $W_{18}O_{49}$ NRs, which acted as support template remained unchanged after Ag/AgCl decoration. Obviously, a number of quasi-spherical nanoparticles (AgCl or Ag or their mixture) with an average diameter of about 40 nm homogeneously decorated on the surfaces of the $W_{18}O_{49}$ NRs. By further observation, a few larger nanoparticles with diameter of up to 100 nm were found, but they also seem anchored strongly on the $W_{18}O_{49}$ NRs surface.

Fig. 2b shows a HRTEM image of the Ag/AgCl/$W_{18}O_{49}$ NRs. The quasi-spherical nanoparticles adhered well to the $W_{18}O_{49}$ NR with clear and clean interface. Interestingly, the nanoparticles seemingly consist of two different components with a distinct interface. The detailed structure and interfacial region of the Ag/AgCl/$W_{18}O_{49}$ NRs was further investigated by enlarged HRTEM images, as shown in Fig. 2c and d. The lattice fringe separations of the $W_{18}O_{49}$ nanorod and the outer component of the nanoparticle are ca. 0.38 and 0.24 nm, corresponding to the (0 1 0) plane of the monoclinic $W_{18}O_{49}$ and (1 1 1) plane of the cubic Ag, respectively.

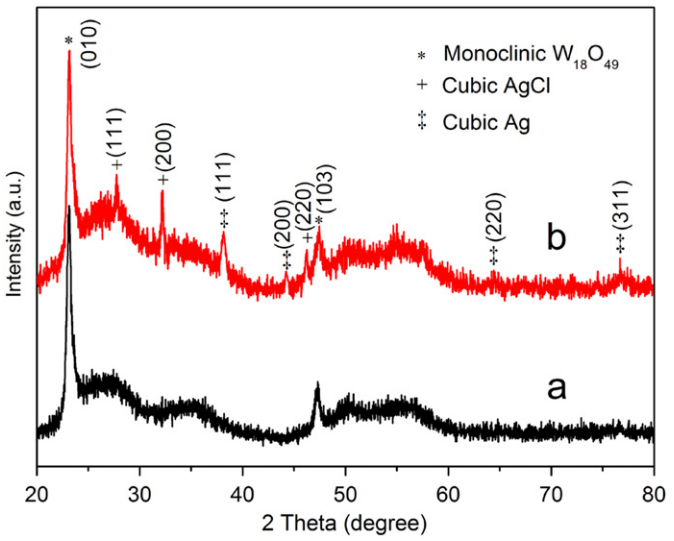

Fig. 1. XRD patterns of (a) $W_{18}O_{49}$ NRs and (b) Ag/AgCl/$W_{18}O_{49}$ NRs.

Herein, it can be confirmed that the outer shell of the nanoparitlces adjoining the $W_{18}O_{49}$ nanorods is Ag, and the interior core is AgCl. The growth direction of the nanorod, *i.e.* [0 1 0] orientation, is perpendicular to the (0 1 0) plane of $W_{18}O_{49}$, in agreement with the XRD result, as shown in Fig. 2d. The Fast Fourier Transform (FFT) pattern of the interface between the $W_{18}O_{49}$ nanorod and the Ag shell shows two sets of diffraction spots: the main one consisting of a series of diffraction spots corresponds to the single-crystalline monoclinic $W_{18}O_{49}$, and the other one consisting of two spots corresponds to the single-crystalline cubic Ag, as shown in Fig. 2e.

The surface characteristics of the Ag/AgCl/$W_{18}O_{49}$ NR have been assessed by XPS, as shown in Fig. 3. The survey XPS spectrum indicates that the elements of W, O, Cl and Ag were detected in the Ag/AgCl/$W_{18}O_{49}$ NRs. No other impurity peaks were detected, evidencing high purity of the resulting products. The carbon peak (C 1s) in the XPS spectra at 285 eV is due to the carbon paste used to stick the samples on the mount. The core-level XPS spectrum of Ag 3*d* could be deconvoluted into two doublets, as shown in Fig. 3b. The main one (dashed lines) consists of two peaks with binding energies of 373.54 and 367.54 eV, which should belong to Ag $3d_{3/2}$ and Ag $3d_{5/2}$ of Ag^{1+} formal oxidation state (AgCl), respectively. The second doublet (dotted lines) has binding energies of 374.43 and 368.44 eV with a spin energy separation of 6.0 eV, corresponding to the metallic Ag [33–35].

3.2. Gas-sensing activities of Ag/AgCl/$W_{18}O_{49}$ NRs sensor

Fig. 4a shows the response curves of the Ag/AgCl/$W_{18}O_{49}$ NRs sensors towards 100 ppm vapors or gases including ethanol, acetone, 93# gasoline, formaldehyde, and NH_3 at an operating temperature of 300 °C. Upon exposure to the detected gases, the output voltage (U_{out}) increased apparently, indicating decreased resistance of the Ag/AgCl/$W_{18}O_{49}$ NRs sensors. This is characteristic of *n*-type semiconductor [36,37]. In addition, the resistance of the Ag/AgCl/$W_{18}O_{49}$ NRs sensors exposing to H_2S decreases with increasing H_2S concentration, as shown in Fig. 4b. It is apparent that the Ag/AgCl/$W_{18}O_{49}$ NRs sensors are highly selective and sensitive to NH_3, acetone and H_2S. As listed in Table 1, the sensitivities of the Ag/AgCl/$W_{18}O_{49}$ NRs sensors to NH_3, acetone and H_2S at 100 ppm are much higher than those to

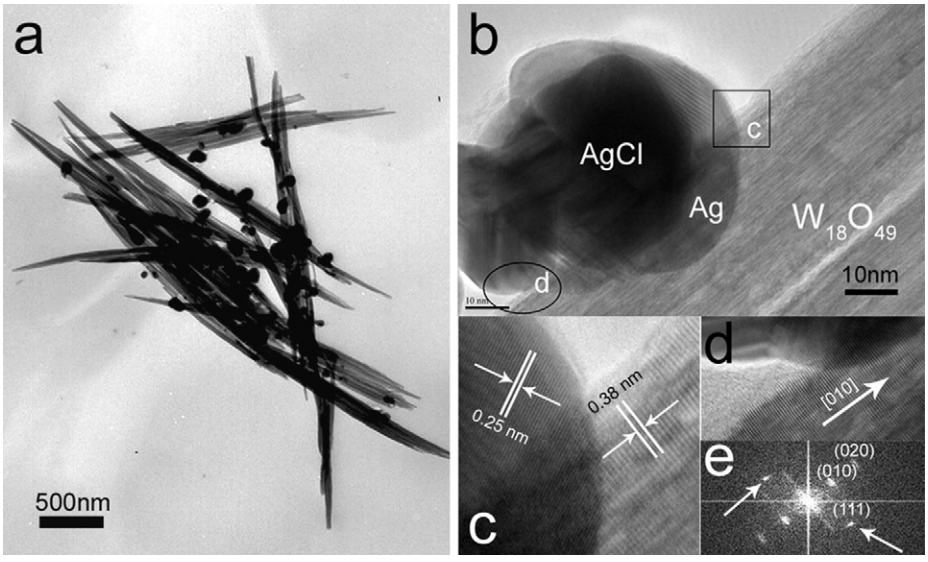

Fig. 2. (a) TEM images of the Ag/AgCl/$W_{18}O_{49}$ NRs; (b) a HRTEM image of the Ag/AgCl/$W_{18}O_{49}$ NR; (c) and (d) enlarged HRTEM of the corresponding area in Fig. 2b; (e) FFT pattern of the interface between the Ag nanoparticle and the $W_{18}O_{49}$ nanorod in (c).

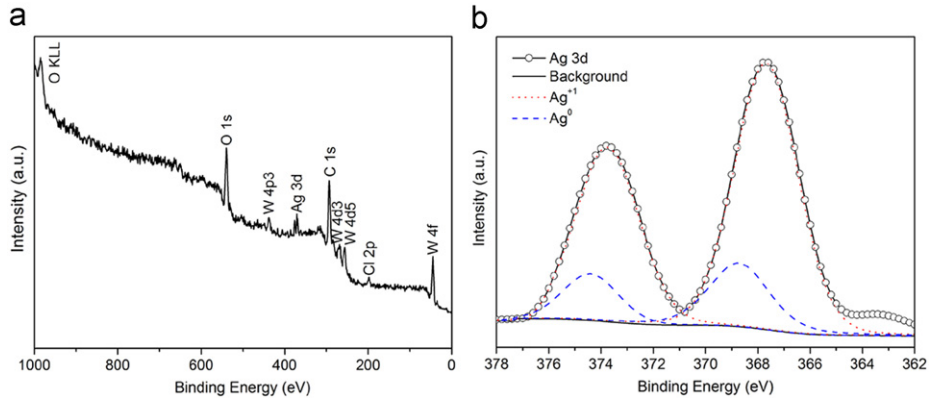

Fig. 3. (a) XPS survey spectra for the Ag/AgCl/$W_{18}O_{49}$ NRs and (b) Ag 3*d* core-level spectrum.

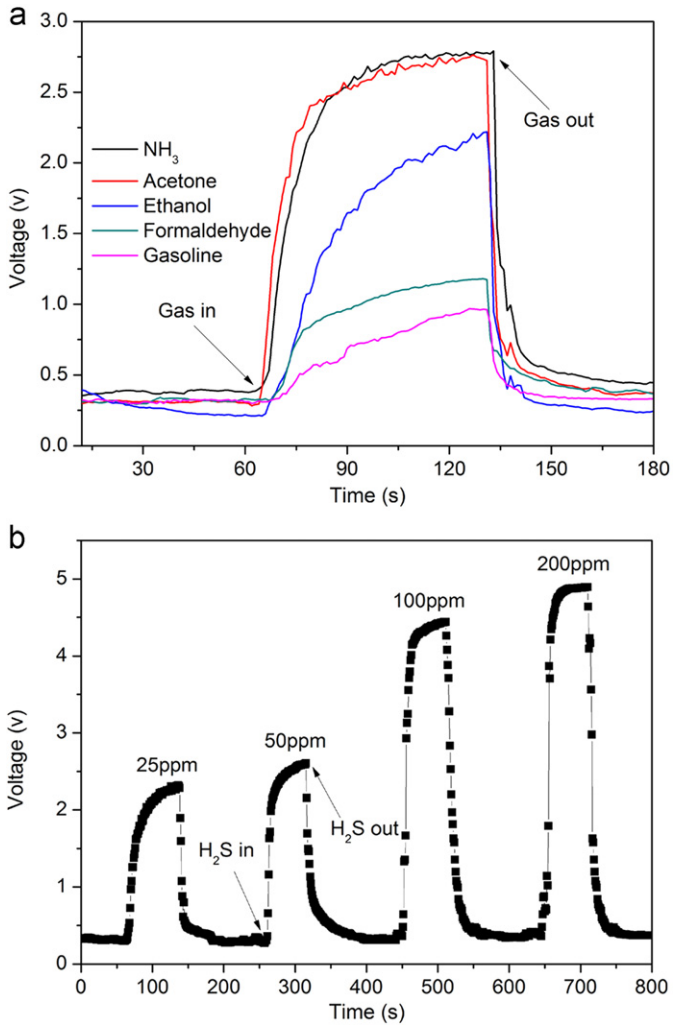

Fig. 4. (a) Typical response curves of the Ag/AgCl/$W_{18}O_{49}$ NRs sensor to various detected vapors or gases of 100 ppm at the operating temperature of 300 °C; and (b) H_2S response curves of the Ag/AgCl/$W_{18}O_{49}$ NRs sensor under different H_2S concentrations at the operating temperature of 300 °C.

ethanol, NO_2 and gasoline. In the case of H_2S, the sensitivity increases from 41.2 at 25 ppm to 60.5 at 50 ppm and 115.5 at 100 ppm. By comparison, the sensitivities of the sensors to formaldehyde and gasoline are lower by two orders of magnitude. When the H_2S concentration is 200 ppm, the output voltage is close to the source voltage (5 V), resulting in an extremely high sensitivity of 594.84.

Table 1
Response time, recovery time and gas sensitivity (R_{air}/R_{gas}) of the Ag/Cl/Ag/$W_{18}O_{49}$ NRs sensors to various gases operated at 300 °C. The sensitivity of bare $W_{18}O_{49}$ NRs was tested for comparison.

Ag/AgCl/$W_{18}O_{49}$	Concentration (ppm)	Response time (s)	Recovery time (s)	Sensitivity	Sensitivity of bare $W_{18}O_{49}$
Ethanol	100	94	45	32.35	13.06
Acetone	100	42	34	66.63	23.32
Gasoline	100	126	51	2.07	–
NH_3	100	45	25	63.82	26.8
NO_2	100	74	48	9.92	8.3
H_2S	25	35	46	41.2	–
H_2S	50	24	41	60.5	–
H_2S	100	21	26	115.5	42.6
H_2S	200	15	28	594.84	–

Response and recovery times are also important parameters for the gas sensors, since rapid reply to target gas are basic demand for practical applications. Both the response and recovery times of the Ag/AgCl/$W_{18}O_{49}$ NRs sensors to 100 ppm ethanol, gasoline and formaldehyde are much longer than those to 100 ppm NH_3, acetone and H_2S. The response and recovery times to H_2S are the shortest among all the tested gases under concentration of 100 ppm at the operating temperature of 300 °C, which are 21 and 26 s, respectively. Increasing the H_2S concentration to 200 ppm, the response time decreases to 15 s.

In order to investigate the effect of Ag/AgCl loading on the gas-sensing properties of $W_{18}O_{49}$ NRs, the sensitivity of bare $W_{18}O_{49}$ NRs were also tested. For the detected vapors or gases of 100 ppm, including ethanol, acetone, NH_3, and H_2S, the sensitivities of the Ag/AgCl/$W_{18}O_{49}$ NRs are much better than those of bare $W_{18}O_{49}$ NRs under the same testing condition, as shown in Table 1. Only for the case of as formaldehyde, the sensitivity of the pure $W_{18}O_{49}$ NRs is comparable to that of the Ag/AgCl/$W_{18}O_{49}$ NRs.

As *n*-type metal-oxide-semiconductor (MOS) sensor, the gas-sensing performance of tungsten oxide sensors is governed by surface-controlled mechanism [38]. Under air atmosphere, adsorbates on the surface of tungsten oxide including O^{2-}, O_2^-, and O^- formed by ambient oxygen capture the electron carriers. Upon exposure to reducing chemicals such as ethanol, acetone, NH_3, etc., the arrested electrons are released by the reactions between the reducing gas and absorbates, leading to the decreased resistance. Conversely, the resistance increases when exposing to oxidizing gases such as NO_2. Since the change of resistance of MOS sensors depend on the species and amount of adsorbates on the surface as well as the electron transfer, both the chemical and electronic sensitization mechanisms could be considered for explaining the enhanced gas-sensing property of

the Ag/AgCl/$W_{18}O_{49}$ NRs sensors. The enhanced gas-sensing activity on the addition of Ag in $SnO_{1.8}$ nanoparticle films has been well explained on the basis of the chemical sensitization due to the spillover effect [37,39]. The similar mechanism also can be employed in the present study. Here, the conductive Ag shell of the Ag/AgCl nanoparticles act as centers for surface–gas adsorption and spill the gas over the $W_{18}O_{49}$ NRs surface via the spillover effect to react with the negative charged chemisorbed oxygen. In the electronic mechanism, the negative charged adsorbates at the Ag/gas interface induces a variation of the surface barrier height, resulting in an electron deficit in the oxide. When the reducing gases is oxidized on the metal surface, an electron is given back to the metal and then to the oxide. Accordingly, the resistance of the semiconductor oxide changes [40,41]. Besides, the influence of Ag/AgCl loading on the gas-sensing performance of Ag/AgCl/$W_{18}O_{49}$ NRs may be related to the oxygen migration between the Ag/AgCl NPs and the $W_{18}O_{49}$ NRs [42].

3.3. Photocatalytic activities of Ag/AgCl/$W_{18}O_{49}$ NRs photocatalyst

Photocatalytic activities of the Ag/AgCl/$W_{18}O_{49}$ NRs photocatalysts were evaluated based on their ability to degrade the methyl orange (MO) solutions under simulated sunlight irradiation. Fig. 5 shows the time course of photocatalytic degradation of MO over the Ag/AgCl/$W_{18}O_{49}$ NRs photocatalysts. For comparison, MO degradation over bare $W_{18}O_{49}$ NRs and Ag/ZnO nanoparticles with diameters of about 20 nm prepared by a coprecipitation method were also measured at the same time. It is obvious that the Ag/AgCl/$W_{18}O_{49}$ NRs exhibits superior photocatalytic activity to those of bare $W_{18}O_{49}$ NRs and Ag/ZnO nanoparticles. After 30 min irradiation by simulated sunlight, the MO degradation efficiency over the Ag/AgCl/$W_{18}O_{49}$ NRs is about 1.5 times and 2.5 times higher than those over the bare $W_{18}O_{49}$ NRs and the Ag/ZnO nanoparticles, respectively. Photocatalytic degradation of MO over the Ag/AgCl/$W_{18}O_{49}$ NRs is almost complete in 90 min. For the case of the bare $W_{18}O_{49}$ NRs and the Ag/ZnO NPs, however, their degradation efficiencies are only 70% and 90% under simulated sunlight irradiation for 150 min. It is noteworthy that the photocatalytic processes of MO over the bare $W_{18}O_{49}$ NRs and the Ag/AgCl/$W_{18}O_{49}$ NRs are similar, during which fast degradation of MO occurred in the first 30 min and then the degradation rate decreased rapidly; while the degradation rate of the Ag/ZnO NPs was almost constant with increasing irradiation time. This may be due to the different structure of the Ag/AgCl/$W_{18}O_{49}$ NRs and the Ag/ZnO NPs.

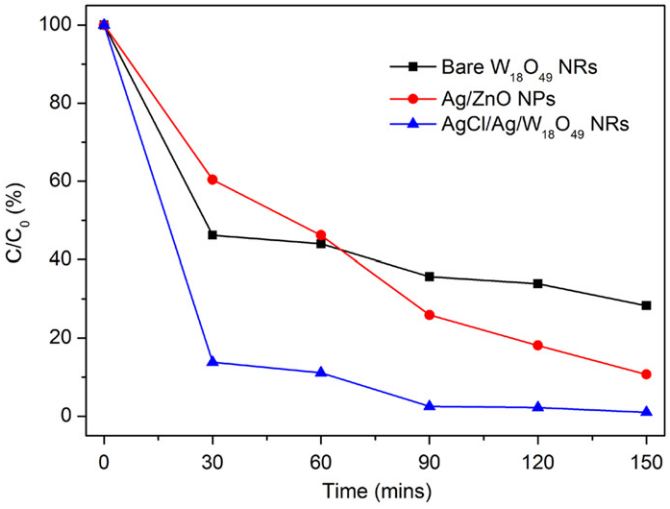

Fig. 5. Photocatalytic degradation of MO using Ag/AgCl/$W_{18}O_{49}$ NRs. Bare $W_{18}O_{49}$ NRs and Ag/ZnO nanoparticles were used as reference samples.

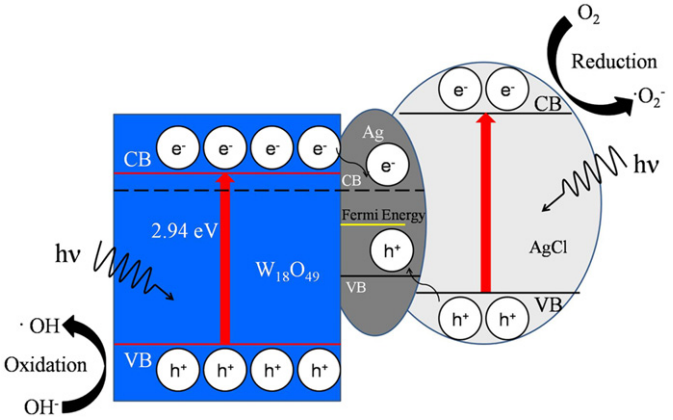

Fig. 6. Schematic illustration of MO degradation over the Ag/AgCl/$W_{18}O_{49}$ NRs photocatalyst.

The photocatalytic mechanism of the Ag/AgCl/$W_{18}O_{49}$ NRs is schematically illustrated in Fig. 6. With energy higher than the band-gap in $W_{18}O_{49}$ and AgCl, band-gap excitation occurred, which leads to the formation of photoexcited holes in the valence band (VB) and photoexcited electrons in the conduction band (CB). The photoelectrons in the CB of $W_{18}O_{49}$ could easily flow into metal Ag through Schottky barrier because of the lower Fermi energy of Ag than the VB level of $W_{18}O_{49}$. Thus, recombination of the electron–hole pairs could be restrained [21,25]. Since the transfer process of photoelectrons from $W_{18}O_{49}$ to Ag is faster than the recombination of electron–hole pairs between the VB and CB of $W_{18}O_{49}$, more holes with strong oxidation power in the VB could be trapped by OH^- to form hydroxyl radicals ($^{\bullet}OH^-$). Meanwhile, the holes in the VB of AgCl can also flow into Ag due to the higher Fermi energy of Ag than the VB level of AgCl. Therefore, more photoelectrons with strong reduction power in the CB of AgCl could reduce absorbed oxygen to form $^{\bullet}O_2^-$. In the photocatalytic process, the metal Ag shell between AgCl core and $W_{18}O_{49}$ nanorods acts as recombination center of the electrons from the CB of $W_{18}O_{49}$ and holes from the VB of AgCl, prohibiting the pair recombinations in both $W_{18}O_{49}$ and AgCl and enhancing the interfacial charge transfer, which is similar to photocatalytic mechanism of the AgBr–Ag–Bi_2WO_6 nanojunction system proposed by Zhang et al. [31]. As a result, electrons form the VB of $W_{18}O_{49}$ and holes from the CB of AgCl can be efficiently generated, leading to the continuous formation of $^{\bullet}O_2^-$ and $^{\bullet}OH^-$ on the surface of Ag/AgCl/$W_{18}O_{49}$ NRs, which would oxide MO at a high photodegradation rate. Furthermore, Ag/AgCl nanoparticles loaded on the $W_{18}O_{49}$ NRs could lonely act as superior visible-light-driven photocatalysts for degrading organic contaminants, further enhancing the photocatalytic activity of the Ag/AgCl/$W_{18}O_{49}$ NRs composite [25,27].

4. Conclusions

In summary, Ag/AgCl nanoparticle decorated $W_{18}O_{49}$ nanorods were prepared by solvothermal method and subsequent photochemical process. After decoration of the nanoparticles consisting of AgCl core and Ag shell, the gas-sensing and photocatalytic properties of the $W_{18}O_{49}$ NRs were apparently enhanced. The Ag/AgCl/$W_{18}O_{49}$ NRs sensors were found to exhibit high sensitivities toward several reducing gases, such as NH_3 (63.82 to 100 ppm), acetone (66.63 to 100 ppm) and H_2S (115.5 to 100 ppm). Chemical and electronic sensitization mechanisms may account for the enhanced gas-sensing property. The Ag/AgCl/$W_{18}O_{49}$ NRs

photocatlysts could decompose methyl orange in aqueous solution at a higher rate than that of bare $W_{18}O_{49}$ NRs under simulated sunlight irradiation. The metal Ag may act as recombination center of the electrons from the CB of $W_{18}O_{49}$ and holes from the VB of AgCl, prohibiting the pair recombinations in both $W_{18}O_{49}$ and AgCl, and finally improving the photocatalytic performance.

Acknowledgment

This work is financially supported by the National Natural Science Foundation of China (50572041), the Application Foundation Research Program of Qingdao (09-1-3-27-jch), the Science & Technology Program of Shanghai Maritime University (20110026), and the Innovative Science and Technology Research Project of Shanghai Education Commission (10ZZ98).

Appendix A. Supporting information

Supplementary data associated with this article can be found in the online version at doi:10.1016/j.jssc.2011.06.024.

References

[1] E. Serrano, G. Rus, J.G. Martinez, Renew. Sust. Energ. Rew. 13 (2009) 2373–2384.
[2] R. Wang, K. Hashimoto, A. Fujishima, Nature 388 (1997) 431–432.
[3] R. Asahi, T. Morikawa, T. Ohwaki, K. Aoki, Y. Taga, Science 293 (2001) 269–271.
[4] J. Wang, S.P. Li, Y.Z. Zhang, Electrochim. Acta 55 (2010) 4436–4440.
[5] Y.F. Hu, J. Zhou, P.H. Yeh, Z. Li, T.Y. Wei, Z.L. Wang, Adv. Mater. 22 (2010) 3327–3332.
[6] Y.R. Zhang, J. Wan, Y.U. Ke, J. Hazard. Mater. 177 (2010) 750–754.
[7] D.L. Chen, X.X. Hou, H.J. Wen, Y. Wang, H.L. Wang, X.J. Li, R. Zhang, H.X. Lu, H.L. Xu, S.K. Guan, J. Sun, L. Gao, Nanotechnology 21 (2010) 035501 12pp.
[8] Y.D. Zhang, Z. Zheng, F.L. Yang, Ind. Eng. Chem. Res. 49 (2010) 3539–3543.
[9] X. Wang, C.G. Hu, H. Liu, G.J. Du, X.S. He, Y. Xi, Sens. Actuators, B 144 (2010) 220–225.
[10] S. Pokhrel, C.E. Simion, V. Quemener, N. Barsan, U. Weimar, Sens. Actuators, B 133 (2008) 78–83.
[11] Y.H. Choi, S.H. Hong, Sens. Actuators, B 125 (2007) 504–509.
[12] C. Balazsi, K. Sedlackova, E. Llobet, R. Ionescu, Sens. Actuators, B 133 (2008) 151–155.
[13] C.S. Rout, M. Hegde, C.N.R. Rao, Sens. Actuators, B 128 (2008) 488–493.
[14] Y.M. Zhao, Y.Q. Zhu, Sens. Actuators, B 137 (2009) 27–31.
[15] X.P. Shen, G.X. Wang, D. Wexler, Sens. Actuators, B 143 (2009) 325–332.
[16] S.B. Sun, X.T. Chang, Z.J. Li, Mater. Res. Bull. 45 (2010) 1075–1079.
[17] T. Arai, M. Yanagida, Y. Konishi, Y. Iwasaki, H. Sugihara, K. Sayama, J. Phys. Chem. C 111 (2007) 7574–7577.
[18] J.Y. Luo, S.Z. Deng, Y.T. Tao, F.L. Zhao, L.F. Zhu, L. Gong, J. Chen, N.S. Xu, J. Phys. Chem. C 113 (2009) 15877–15881.
[19] Z.G. Zhao, M. Miyauchi, Angew. Chem. Int. Ed. 47 (2008) 7051–7055.
[20] R. Abe, H. Takami, N. Murakami, B. Ohtani, J. Am. Chem. Soc. 130 (2008) 7780.
[21] Q. Xiang, G.F. Meng, H.B. Zhao, Y. Zhang, H. Li, W.J. Ma, J.Q. Xu, J. Phys. Chem. C 114 (2010) 2049–2055.
[22] H.J. Xia, Y. Wang, F.H. Kong, S. Wang, B.L. Zhu, X.Z. Guo, J. Zhang, Y.M. Wang, S.H. Wu, Sens. Actuators, B 134 (2008) 133–139.
[23] S.M. Sun, W.Z. Wang, S.Z. Zeng, M. Shang, L. Zhang, J. Hazard. Mater. 178 (2010) 427–433.
[24] L. Wang, A. Teleki, S.E. Pratsinis, P.I. Gouma, Chem. Mater. 20 (2008) 4794–4796.
[25] P. Wang, B.B. Huang, X.Y. Qin, X.Y. Zhang, Y. Dai, J.Y. Wei, M.H. Whangbo., Ag@AgCl: a highly efficient and stable photocatalyst active under visible light, Angew. Chem. Int. Ed. 47 (2008) 7931–7933.
[26] P. Wang, B.B. Huang, Q.Q. Zhang, X.Y. Zhang, X.Y. Qin, Y. Dai, J. Zhan, J.X. Yu, H.X. Liu, Z.Z. Lou, Highly efficient visible light plasmonic photocatalyst Ag@Ag(Br, I), Chem. Eur. J. 16 (2010) 10042–10047.
[27] C.H. An, S. Peng, Y.G. Sun, Facile synthesis of sunlight-driven AgCl:Ag plasmonic nanophotocatalyst, Adv. Mater. 22 (2010) 2570–2574.
[28] P. Wang, B.B. Huang, X.Y. Qin, X.Y. Zhang, Y. Dai, M.H. Whangbo., Ag/AgBr/$WO_3 \cdot H_2O$: visible-light photocatalyst for bacteria destruction, Inorg. Chem. 48 (2009) 10697–10702.
[29] J.G. Yu, G.P. Dai, B.B. Huang, Fabrication and characterization of visible-light-driven plasmonic photocatalyst Ag@AgCl/TiO_2 nanotube arrays, J. Phys. Chem. C 113 (2009) 16394–16401.
[30] P. Wang, B.B. Huang, X.Y. Qin, X.Y. Zhang, Y. Dai, M.H. Whangbo, Inorg. Chem. 48 (2009) 10697–10702.
[31] L.S. Zhang, K.H. Wong, Z.G. Chen, J.C. Yu, J.C. Zhao, C. Hu, C.Y. Chan, P.K. Wong, Appl. Catal. A—Gen. 363 (2009) 221–229.
[32] S.B. Sun, Y.M. Zhao, Y.D. Xia, Z.D. Zou, G.H. Min, Y.Q. Zhu, Nanotechnology 19 (2008) 305709 7pp.
[33] W. Kwoka, L. Ottaviano, M. Passacantando, G. Czempik, S. Santucci, J. Szuber, Appl. Surf. Sci. 254 (2008) 8089–8092.
[34] H. Zhang, G. Wang, D. Chen, X.J. Lv, J.H. Li, Chem. Mater. 20 (2008) 6543–6549.
[35] P. Wang, B.B. Huang, Z.Z. Lou, X.Y. Zhang, X.Y. Qin, Y. Dai, Z.K. Zheng, X.N. Wang, Chem. Eur. J. 16 (2010) 538–544.
[36] D.E. Williams, P.T. Moseley, J. Mater. Chem. 1 (1991) 809–814.
[37] R.K. Joshi, F.E. Kruis, Appl. Phys. Lett. 89 (2006) 153116 3pp.
[38] M. Feng, A.L. Pan, H.R. Zhang, Z.A. Li, F. Liu, H.W. Liu, D.X. Shi, B.S. Zou, H.J. Gao, Appl. Phys. Lett. 86 (2005) 141901 3pp.
[39] N. Yamazoe, Sens. Actuators B 5 (1991) 7–19.
[40] P. Montmeat, J.C. Marchand, R. Lalauze, J.P. Viricelle, G. Tournier, C. Pijolat, Sens. Actuators B 95 (2003) 83–89.
[41] R.K. Joshi, Q. Hu, F. Alvi, N. Joshi, A. Kumar, J. Phys. Chem. C 113 (2009) 16199–16202.
[42] L. Chen, S.C. Tsang, Sens. Actuators B 89 (2003) 68–75.